

Free volume distribution of nearly jammed hard sphere packings

Moumita Maiti* and Srikanth Sastry†

Jawaharlal Nehru Centre for Advanced Scientific Research, Jakkur Campus, Bangalore 560 064, India and
TIFR Centre for Interdisciplinary Sciences, 21 Brundavan Colony, Narsingi, 500075 Hyderabad, India

We calculate the free volume distributions of nearly jammed packings of monodisperse and bidisperse hard sphere configurations. These distributions differ qualitatively from those of the fluid, displaying a power law tail at large free volumes, which constitutes a distinct signature of nearly jammed configurations, persisting for moderate degrees of decompression. We reproduce and explain the observed distribution by considering the pair correlation function within the first coordination shell for jammed hard sphere configurations. We analyze features of the equation of state near jamming, and discuss the significance of observed asphericities of the free volumes to the equation of state.

Disordered, structurally arrested forms of matter arise through a variety of processes, such as the glass transition in dense, cold liquids, gelation, jamming in granular matter, to name a few examples[1–4]. The nature of these processes and their interrelation are topics of considerable current research activity. Much of the interest is focussed on understanding the manner in which the relaxation dynamics and transport properties change in the fluid state upon approaching the arrest transition. Temperature, density and applied stress are involved as control parameters that determine the transition from an arrested to a fluid state in different systems, and a unified *jamming phase diagram* has been discussed as a possible description of the arrested-to-fluid transition [5]. Recent theoretical work, however, draws a distinction between the glass and jamming transitions (summarized, *e. g.* in [6]), and the exact relationship between these transitions is a topic of ongoing research.

Considerable work addressing the nature of the jamming transition has focussed on packings of hard spheres, dating back to the seminal work of Bernal and co-workers [7, 8], who identified a *random close packing* (RCP) of spheres with a packing fraction of 64%, attained as the maximum density for amorphous packings of equal sized spheres (we express density values in packing fractions throughout). Considering the hard sphere fluid as the initial, thermodynamic equilibrium state from which jammed configurations are generated, RCP would represent a limit state at which the pressure would diverge. While such a point would correspond to a state of structural arrest, many studies suggest that a *glass* transition precedes jamming, at finite pressure [6, 9–12]. Further, in analogy with the glass transition, it has been suggested

and demonstrated that the jamming transition too does not occur at a unique point but can occur over a range of densities [10, 11, 13, 14].

In addition to such analyses concerned with thermodynamic and dynamic (or kinetic) aspects, much attention has been focussed on geometric features of jammed configurations [15–23] (in contrast to the relatively scant attention to structure in the context of glass formation). From such a geometric point of view, the proposal of a unique random close packing has been questioned [15], and it has been proposed that a more suitable notion is that of maximally random jammed packings. Although the jamming density itself is not unique, interestingly, many geometric features remain robust [13]. An important example is the power law singularity in the pair correlation function near contact, observed in addition to the delta function at contact [17–19, 21, 24]. The origins and consequences of these unique geometric features are of considerable current interest.

One of the important ways of characterizing the geometry of hard sphere packings is the distribution of free volumes [25, 26]. The free volume, defined as the volume available to the centre of a hard sphere while all other spheres remain fixed, is further directly related to the equation of state (EOS) [27],

$$\frac{P}{\rho k_B T} = 1 + \frac{\sigma}{2D} \left\langle \frac{s_f}{v_f} \right\rangle, \quad (1)$$

where P is the pressure, T is the temperature, σ the diameter of the spheres, D is the spatial dimensionality ($D = 3$ for all the results shown in this work.), v_f and s_f are respectively the free volume and the surface area of the free volume. An exact algorithm for determining the volume and surface area of cavities in polydisperse sphere packings, developed in [28] has been employed [25, 26] to study free volume distributions in (monodisperse and bidisperse) hard sphere fluids.

*Electronic address: maiti@theorie.physik.uni-goettingen.de;
Present Address: Institute for theoretical Physics, University of Goettingen, Germany.

†Electronic address: sastry@jncasr.ac.in

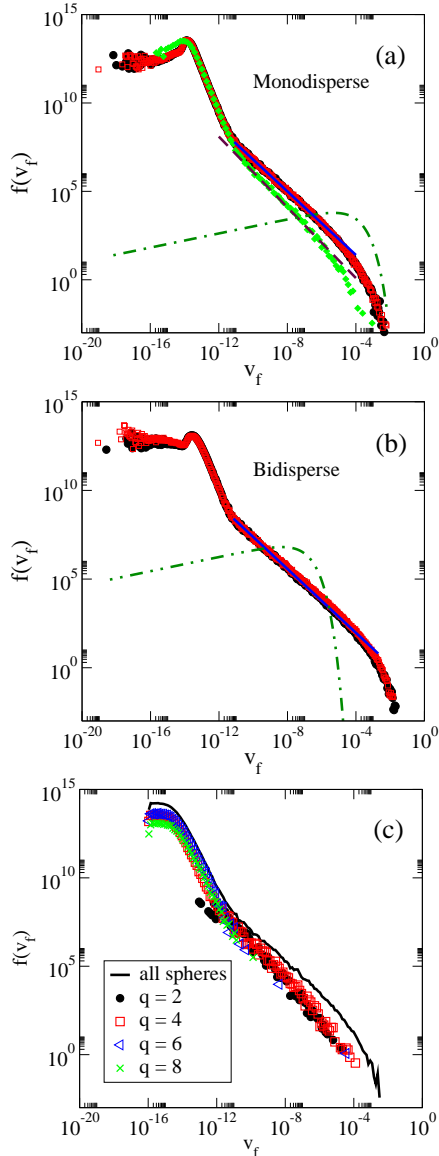


FIG. 1: Free volume distributions for (a) monodisperse (circles: $\phi_{init} = 0.4487$; squares: $\phi_{init} = 0.533$) and (b) (component 1 of the) bidisperse sphere packings ((circles: $\phi_{init} = 0.363$; squares: $\phi_{init} = 0.5919$) close to the jamming point, for the cases listed in tables I and II. Free volume distributions of both packings have a power law tail of exponent -0.9 (solid lines). The distributions are the same regardless of the jamming density. The expected free volume distributions, based on extrapolating (by a polynomial fit to the parameters in Eq. 2 and extrapolating them to the jamming density) those for the fluid (dot dashed lines), are shown for comparison. The distribution obtained without considering the free volumes of rattlers is also shown in (a) for one case ($\phi_{init} = 0.4487$) (diamonds), with a power law tail with exponent -1 (dashed line). (c) Free volume distributions for monodisperse spheres with selected numbers of contact neighbors, $q = 2, 4, 6, 8$, for $\phi_{init} = 0.4487$.

A *cavity* is a connected subset of the void space, which is defined as the volume that lies outside the union of spheres that define the system under consideration. For defining the free volumes, one considers *exclusion spheres* located at the coordinates of each hard sphere, with radius equal to the radius of the hard sphere *plus* the radius of the sphere whose free volume one wishes to compute. Given a configuration of N hard spheres, the free volume of a given hard sphere is the volume of the *cavity* in which its coordinates lie, in a configuration of $N - 1$ spheres excluding the sphere under consideration. The algorithm for computing cavity volumes, described in detail in [26, 28], involves the following steps, for the calculation of free volumes in hard sphere configurations: (i) A Voronoi or generalized Voronoi (radical plane) construction. (ii) Identification of cavities based on connected Voronoi vertices that lie in the void space. (iii) Identification of the set of Delaunay tetrahedra that enclose a given cavity. (iv) Computation of the cavity volume and surface area of the cavity contained in each Delaunay tetrahedron. An efficient way of implementing this algorithm to the free volume calculation without repeated tessellations is described in [25, 26].

The free volume distributions, over a wide range of densities [25, 26], is described well by the form

$$f(v_f) \propto v_f^\alpha \exp(-\beta v_f^\gamma) \quad (2)$$

where the parameters α , β and γ are smoothly varying functions of density yielding a mean free volume that decreases with density. Strictly at the jamming point, the free volumes must equal zero, if one excludes 'rattlers', which are spheres with the number of contacts $q \leq 3$, and are therefore free to move in some directions without hindrance from the contact neighbors. However, slightly below the jamming point, the free volumes are finite, and it is natural to ask what the free volume distributions look like at such densities close to jamming. We address this question in this paper, by generating jammed configurations of monodisperse and bidisperse hard spheres, and calculating the free volume distributions of nearly jammed configurations obtained by decompressing them slightly.

We generate jammed configurations following the procedure in [13, 29], wherein starting from an equilibrated hard sphere fluid at initial density ϕ_{init} , a fast initial compression is effected using a Monte Carlo simulation till the pressure reaches 10^3 (reduced units are used throughout). The system is next treated as made of soft spheres [30] (with interaction potential $V_{\alpha\beta} = (1 - \frac{r_{ij}}{\sigma_{\alpha\beta}})^2$ for $r_{ij} \leq \sigma_{\alpha\beta}$; $= 0$ for $r_{ij} > \sigma_{\alpha\beta}$, where α, β represent different sizes of spheres i, j), and compressed further, till the energy per particle is 10^{-5} . The system is then decompressed in steps, following energy minimization at each step. A jammed configuration (and jamming den-

sity (ϕ_J) is identified by the condition that the single particle energy reaches $e = 10^{-16}$ or smaller. For data shown in figures 1 and 2, the jammed configurations are generated with a tolerance in packing fraction of 10^{-5} , and for figures 4 and 5, 10^{-8} (based on the decompression steps used). We note that we consider only energy minimum structures throughout this procedure, and dynamical effects that may matter in real systems do not play a role in determining the jammed configurations.

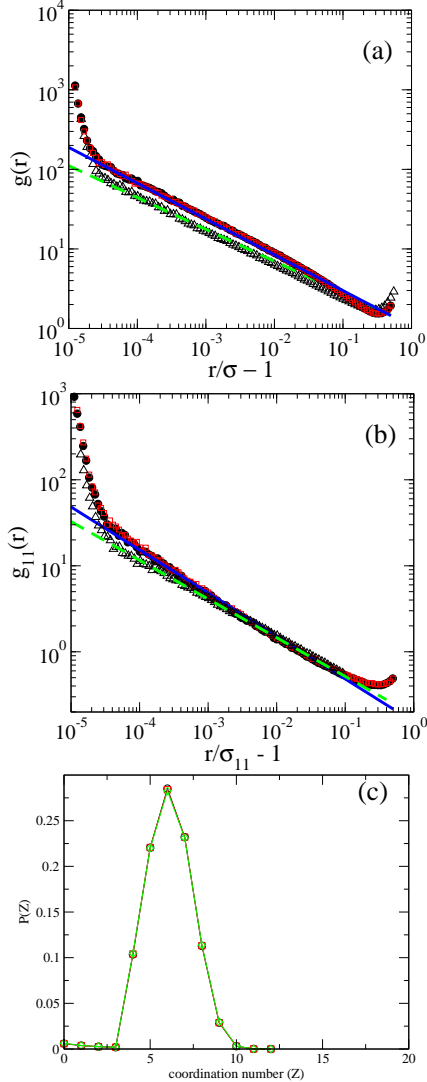


FIG. 2: Pair correlation function $g(r)$ for (a) mono and (b) (component 1 of the) bidisperse sphere packings for the cases shown in Fig. 1. Power law fits close to contact are shown, with exponent -0.45 for mono-disperse packings and -0.5 for the bidisperse packings. $g(r)$ calculated excluding rattlers is also shown (open triangles) along with power law fit lines (dashed lines) for comparison. (c) The distribution of the number of contact neighbors for the mono-disperse case.

We study mono-disperse and bi-disperse hard sphere systems of size $N = 2000$. The bi-disperse system is a 50:50 mixture of spheres of diameter σ (component 1) and 1.4σ (component 2). We choose three initial densities for the mono-disperse fluid, which are smaller than the packing fraction (0.545) of spontaneous crystallization. Four different initial fluid densities of bi-disperse hard spheres are chosen. The jammed densities are evaluated after averaging over 500 (100) independent configurations for figures 1,2 (figures 4,5), ensuring lack of crystallinity through a calculation of orientational order parameters. The statistics of jammed densities for different initial fluid densities are shown in the table I(mono-disperse) and table II(bi-disperse).

ϕ_{init}	$\sim \phi_J(e \leq 10^{-16})$	Rattlers
0.533	0.6419	1.6%
0.4487	0.6394	1.7%
0.2841	0.6392	1.7%

TABLE I: Statistics of jammed configurations of mono-disperse spheres for system size $N = 2000$. ϕ_{init} , ϕ_J are the initial and jammed configuration densities, and e is the energy per particle. Rattlers are spheres with number of contacts $q \leq 3$.

ϕ_{init}	$\sim \phi_J(e \leq 10^{-16})$	Rattlers
0.5919	0.6605	6.1%
0.5704	0.6554	5.6%
0.5396	0.6498	4.9%
0.363	0.6476	4.6%

TABLE II: Statistics of jammed configurations of bi-disperse spheres for system size $N = 2000$. Symbols as in table I.

We calculate the distribution of free volumes, using the algorithm described in [25, 26], for configurations that are decompressed (by 10^{-8} in packing fraction) from the jammed configurations and thermalized by performing a short Monte Carlo simulation of 1000 attempted random displacements (of magnitude comparable to the distance created between contact neighbors by the decompression) per sphere. By extrapolating the parameters of Eq. 2, one may expect a very narrow free volume distribution near the jamming point. Fig. 1 shows the free volume distribution near jamming for both the mono-disperse and bi-disperse packings. In addition to a peak at small free volumes, the distribution displays an unexpected power law tail ($\approx v_f^{-\delta}$), over eight orders of magnitude of free volumes. For both mono- and (both components of the) bi-disperse packings, the exponent

$\delta = -0.9$. These distributions, which are very different from the extrapolation from the fluid state, do not depend on the jamming density. We verify that the tail is not due to rattlers. As shown in Fig. 1 (a), eliminating rattlers from consideration alters the exponent in the power law but does not eliminate the feature. We also verify that the Lubachevsky-Stillinger procedure[31] for generating jammed configurations also produces the power law tail. As supported by results discussed below, the observed power law tail is thus a structural signature of nearly jammed particle packings.

Since the free volume of a sphere is determined by the location of its neighbors, the power law in the free volume distribution may be related to the pair correlation function $g(r)$, which, in addition to a delta function at contact, has a well-studied singularity near contact, $g(r) \approx (\frac{r}{\sigma} - 1)^{-\eta}$ [13, 17, 19, 21, 24] for jammed configurations. The connection is not straight-forward, since $g(r)$ is a two-body property, whereas the free volume of a sphere is a many-body property that depends on the positions of all its neighbors. Further, it is reasonable to expect, as indeed generally done, that the contact neighbors bound the (compact) free volume of a sphere in slightly decompressed configurations. The possibility that non-contact neighbors may play a role at all is therefore suggested by our surprising finding of a large free volume tail, which we explore. As a preliminary test, we compute the free volume distribution for groups of spheres each of which has a particular number of contact neighbors (we discuss the distribution of contact numbers further below). These partial distributions are shown in Fig. 1(c), for contact number $q = 2, 4, 6, 8$. While for $q = 6, 8$ the partial distributions are confined to be small free volume peak, for $q = 2, 4$, one has a substantial contribution in the tail. Thus, the number of contact neighbors plays a crucial role in determining the free volumes, and for contact neighbors less than 6, the free volumes are significantly distributed in the tail.

In Fig. 2 (a) and (b) we show the $g(r)$, which exhibits a power law regime near contact with exponent value $\eta = -0.45$ for monodisperse packings and $\eta = -0.5$ for component 1 of the bidisperse case. As discussed previously [17, 19, 24], and we show in Fig. 2, the $g(r)$ exponent depends whether rattlers are included in its evaluation or not. We analyze configurations which include rattlers, and choose the distance at which $g(r)$ deviates from the power law, ($\approx 10^{-5}$), as the cutoff to identify contact neighbors. The distribution of the number of contact neighbors is shown in Fig. 2(c) for the monodisperse case. Interestingly, roughly a third of the spheres have less than 6 contact neighbors, and thus the spheres whose free volumes may contribute to the tail of the distribution is not a negligible fraction. We note that the population with $q \leq 3$ (*i. e.* rattlers) are expected to

have $q = 0$ with a precise definition of contact neighbors, and indeed find that the population of spheres with $q = 1, 2, 3$ decreases with an increase in the precision with which contact neighbors are identified.

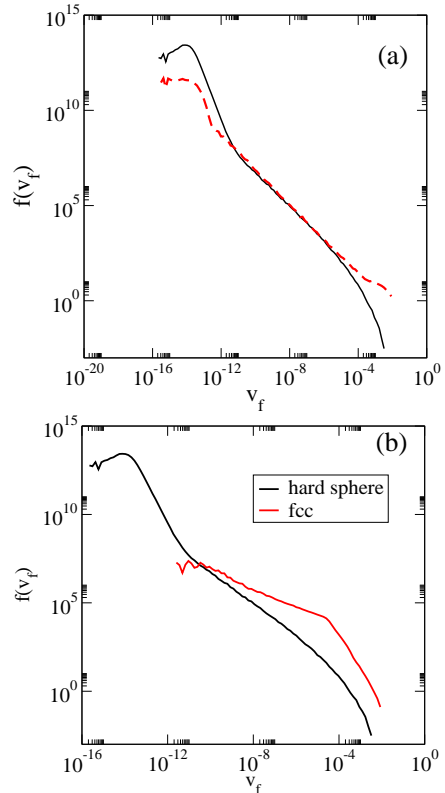


FIG. 3: (a) Comparison of the free volume distribution of monodisperse sphere packings (solid line) with the *icosahedron model*. (dashed line). (b) Comparison of the free volume distribution of monodisperse sphere packings (solid line) with the model calculation wherein the neighbors occupy nearest neighbor positions in the FCC lattice.

We next consider a *toy* computation wherein the free volume of a sphere in the centre of an icosahedral cluster of spheres is considered. Starting with a regular, compact configuration, the 12 spheres on the periphery are displaced according to the distribution of neighbor distances observed for monodisperse packings. As shown in Fig. 3 (a), the free volume distribution for the *icosahedron model* indeed displays a power law tail, with the correct exponent, though it is too simple a model to capture all relevant details accurately, such as the relative amplitudes of the peak and the power law tail. Choosing initial neighbor positions arranged in an *FCC* configuration, rather than an icosahedron, leads to a distribution with different features and a different exponent for its tail, as shown in Fig. Fig. 3 (b) These observations, suggest

that the free volume distribution depends sensitively on the many body correlations of neighbor positions, which needs further analysis to elucidate.

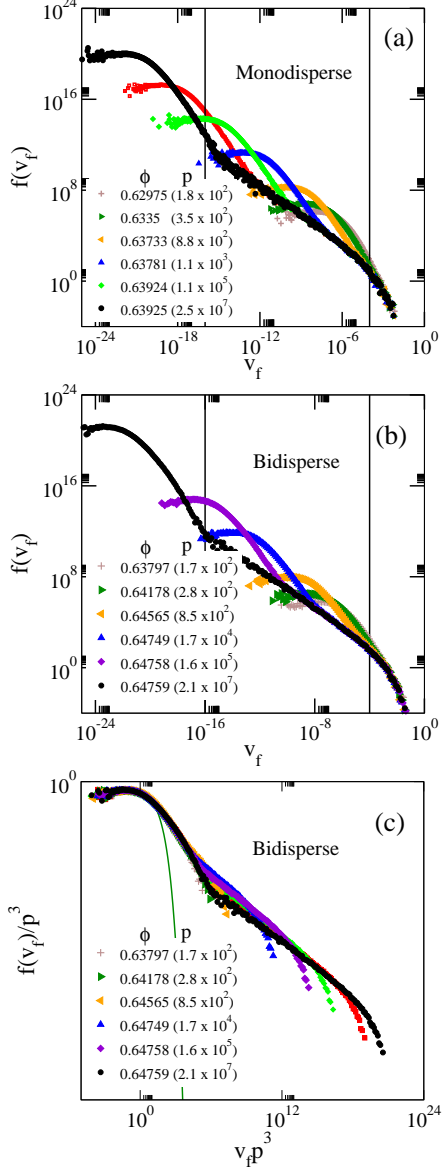


FIG. 4: Evolution of the free volume distribution of (a) monodisperse and (b) (component 1 of the) bidisperse sphere packings, upon decompression. Distributions for the bidisperse case have been scaled with p^3 in (c) ($p = \frac{P}{\rho k_B T} - 1$) to emphasize that invariant shape of the peak of the distributions, which is significantly broader than for the liquid (Eq. 2 and Fig. 1; solid line). The densities ϕ and p of (some of) the decompressed configurations are shown in the legends. Vertical lines in panel (a) indicate the range of v_f over which one observes the power law tail for the highest density in both the cases.

We next consider the manner in which the free volume distribution evolves upon decompression. To do so, the sizes of the spheres are rescaled to correspond to a range of densities lower than the jamming density, and the configurations are thermalized by performing short Monte Carlo simulations (see above) at each density. As shown in Fig. 4 (a) and (b), the distributions evolve towards those found in the liquid state, but interestingly, the power law tail persists over a finite range of densities.

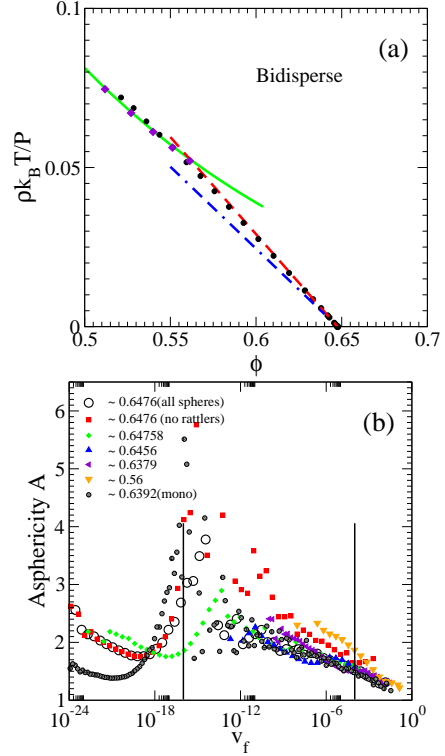


FIG. 5: (a) The equation of state (EOS) near jamming of bidisperse system. The solid line represents the Carnahan-Starling (CS) EOS. Also shown (diamonds) are pressures for the fluid obtained from Eq. 1. The data points from decompressed configurations are fit to the form 3 with $C = 2.53$ (dashed lines) with an intersection with the CS EOS at $\phi = 0.562$. The line with $C = D$ is also shown for reference (dot dashed lines). (b) Asphericity A (see text) shown for bidisperse configurations for a range of densities. Asphericities for the monodisperse case, and the fluid ($\phi = 0.56$) are shown for comparison.

We use the configurations generated above to calculate the pressures, using Eq. 1. The EOS near the jamming point predicted by Salsburg and Wood [32], obtained by assuming compact free volumes,

$$\frac{P}{\rho k_B T} = \frac{C\phi_J}{\phi_J - \phi}; C = D. \quad (3)$$

This prediction has been verified [17] in earlier work but for configurations without rattlers. Speedy [33] reported $C = 2.67$ for monodisperse hard spheres. As discussed in [17, 34], the presence of rattlers will reduce the value of C linearly with the fraction of rattlers. However, our results for the bidisperse system, shown in Fig. 5(a), consistent with a value of $C = 2.53$, cannot be explained by the presence of rattlers alone (see Table II, $\phi_{init} = 0.363$. Rattler fraction $f = 4.6\%$ implies $C = D(1 - f) = 2.862$), and must also have a contribution from free volume heterogeneity [17, 34]. As can be seen from Fig. 4(c), the peak of the free volume distribution, plotted against free volume scaled by p^3 (based on $p \sim 1/\delta$, $v_f \sim \delta^3$ where δ is the distance to the contact neighbors) has a density invariant shape that is significantly broader than the form obeyed by the liquid. We also calculate the asphericity A of free volumes, defined as $A = \frac{1}{2D} \frac{s_f}{v_f^{2/3}}$ ($A = 0.806$ for spherical and $= 1$ for a cubic free volumes). As shown in Fig. 5(b), free volumes over the full range of values show asphericity to varying degrees, for different degrees of decompression, with the asphericities being maximum in the initial part of the power law tail in all cases. The role played by these two factors merits further investigation. It is interesting to note that the intersection of the free volume EOS Eq. 3 with the fluid (CS) EOS occurs around 0.562, close to the experimental number of 0.58 for the glass transition as described by mode coupling theory. Since the EOS Eq. 3 is

obtained for jammed configurations decompressed with a very short equilibration time, it is interesting to interpret the intersection density of 0.562 as the limiting density for the glass in the limit of infinitely fast decompression, which has consistency with the emergence of the mode coupling transition as a limit of stability in some descriptions of the glass transition [35]. It should be observed that the intersection density would be very much lower if $C = D$. Thus, the presence of rattlers and free volume anisotropies seem to have a role in determining a meaningful transition density from the glass to the fluid states.

In summary, we have calculated free volume distributions for nearly jammed sphere packings, and show that they exhibit a characteristic power law tail, which we show is related to the power law singularity in the pair correlation function. The power law tail persists for moderate degrees of decompression and are thus a signature of packing close to jamming. We show evidence that the deviations of the equation of state close to jamming from the prediction for ideal jammed packings arise from the asphericities of the free volumes in addition to the presence of rattlers.

I. ACKNOWLEDGEMENTS:

We wish to thank Salvatore Torquato, Francesco Zamponi, Giorgio Parisi, Patrick Chabonnet, Gilles Tarjus and Sidney Nagel for useful discussions.

-
- [1] P. G. Debenedetti, *Metastable Liquids: Concepts and Principles* (Princeton University Press, 1996).
 - [2] K. Binder and W. Kob, *Glassy Materials and Disordered Solids: An Introduction to their Statistical Mechanics*, (World Scientific, 2005).
 - [3] *Dynamical Heterogeneities in Glasses, Colloids, and Granular Media*, L. Berthier, *et al.*, eds. (Oxford University Press, 2011)
 - [4] S. Torquato, *Random Heterogeneous Materials: Microstructure and Macroscopic Properties* Springer-Verlag (2002).
 - [5] A. J. Liu and S. R. Nagel, *Nature* **396**, 21 (1998).
 - [6] G. Parisi and F. Zamponi, *Rev. Mod. Phys.* **82**, 789 (2010).
 - [7] J. D. Bernal, *Nature* **185**, 68 (1960)
 - [8] J. D. Bernal and J. Mason, *Nature* **188**, 910 (1960).
 - [9] R. J. Speedy, *J. Chem. Phys.* **100** 6684 (1994).
 - [10] R. J. Speedy, *Mol. Phys.* **95** 169 (1998).
 - [11] F. Krzakala and J. Kurchan, *Phys. Rev. E* **76**, 021122 (2007).
 - [12] G. Parisi and F. Zamponi, *J. Chem. Phys.* **123**, 144501 (2005).
 - [13] P. Chaudhuri, L. Berthier, and S. Sastry, *Phys. Rev. Lett.* **104**, 165701 (2010).
 - [14] Y. Jiao, F. H. Stillinger, and S. Torquato, *J. Appl. Phys.* **109**, 013508 (2011).
 - [15] S. Torquato, T. M. Truskett, and P. G. Debenedetti, *Phys. Rev. Lett.* **84**, 2064 (2000).
 - [16] S. Torquato and F. H. Stillinger, *Rev. Mod. Phys.* **82**, 26332672 (2010).
 - [17] A. Donev, S. Torquato, and F. H. Stillinger, *Phys. Rev. E* **71**, 011105 (2005).
 - [18] C. S. O'Hern, L. E. Silbert, A. J. Liu and S. R. Nagel, *Phys. Rev. E* **68**, 011306 (2003).
 - [19] L. E. Silbert, A. J. Liu, and S. R. Nagel, *Phys. Rev. E* **73**, 041304 (2006).
 - [20] M. Clusel, E. I. Corwin, A. O. N. Siemens, J. Brujic, *Nature* **460**, 611 (2009).
 - [21] M. Wyart, *Phys. Rev. Lett.* **109**, 125502 (2012).
 - [22] A. B. Hopkins, F. H. Stillinger, and S. Torquato, *Phys. Rev. E* **86**, 021505 (2012).
 - [23] V. Ogarko, N. Rivas and S. Luding, *J. Chem. Phys.* **140**, 211102 (2014).
 - [24] P. Charbonneau, E. I. Corwin, G. Parisi and F. Zamponi, *Phys. Rev. Lett.* **109** 205501 (2012).
 - [25] S. Sastry, T. M. Truskett, P. G. Debenedetti, S. Torquato and F. H. Stillinger, *Mol. Phys.* **95**, 289 (1998).
 - [26] M. Maiti, A. Lakshminarayanan, S. Sastry, *Eur. Phys. J.*

- E.* **36**:5 (2013).
- [27] R. J. Speedy, *J. chem. Soc. Faraday Trans II* **76**, 693 (1980).
- [28] S. Sastry, D. S. Corti, P. G. Debenedetti and F. H. Stillinger, *Phys. Rev. E* **56**, 5524, (1997).
- [29] L. Berthier and T. A. Witten, *Phys. Rev. E* **80**, 021502 (2009).
- [30] C. S. O'Hern, S. A. Langer, A. J. Liu, and S. R. Nagel, *Phys. Rev. Lett.* **88**, 075507 (2002).
- [31] B. D. Lubachevsky and F. H. Stillinger, *J. Stat. Phys.* **60**, 561 (1990).
- [32] Z. W. Salsburg and W. W. Wood, *J. Chem. Phys.* **37**, 798(1962).
- [33] R. J. Speedy, *Mol. Phys.* **83**, 591 (1994).
- [34] P. Charbonneau, A. Ikeda, G. Parisi and F. Zamponi, *Phys. Rev. Lett.* **107** 185702 (2011).
- [35] S. Franz and G. Parisi, *Phys. Rev. Lett.* **79**, 2486(1997).